Investigation of rotorcraft-pilot couplings under flight-path constraint below the minimum-power speed

L. Lu
Linghai@liv.ac.uk
G.D. Padfield and M. Jump
Flight Science and Technology Research Group, Department of Engineering
University of Liverpool, the Quadrangle
Liverpool
UK

ABSTRACT

In some situations, closed loop control by the pilot can result in the combined pilot-aircraft system becoming marginally stable or even unstable. This can happen whether the pilot is controlling attitude or flight path. In this paper, an investigation into helicopter stability under flight-path constraint below the minimum-power speed is reported. The work provides a theoretical basis for flight path handling qualities criteria particularly for flight on the, so-called, back-side of the power curve. The research uses the theory of weakly coupled systems by partitioning the helicopter longitudinal dynamics to investigate three interacting subsystems – classically the surge mode, the phugoid mode and the heave mode. Under certain conditions, strong control of flight path or vertical speed is shown to drive the aircraft-pilot system unstable and a conflict is shown to exist between feedback gain values to guarantee stability of both the surge and the flight path motions. This conflict constitutes a potential source of adverse rotorcraft-pilot couplings. The problems are exacerbated in cases when the use of collective control is restricted. The phenomenon is explored in both ground based simulation and flight test to provide a verification of the theory.

NOMENCLATURE

$\mathbf{A}, \mathbf{A}_{i,j}$	system matrix and its sub-partitioning
g	gravitational acceleration, ft/s^2
k_{max}	maximum gain value for loci plot
K_{V_x}, K_{V_z}	feedback gains from inertial horizontal and vertical velocities to longitudinal cyclic
K_{w0}	feedback gain from vertical velocity to longitudinal cyclic
$K_{1\text{-}3}$	critical gains for phugoid mode
l, m	orders of matrix $\mathbf{A}$ and $\mathbf{A}_{11}$, respectively
M_q, M_u, M_w	pitch moment derivatives
M_η, $M_{\theta_{is}}$	control derivatives
n	order of matrix $\mathbf{A}_{22}$
q	pitch rate
r, R	maximum and minimum moduli of eigenvalues of $\mathbf{A}_{11}$ and $\mathbf{A}_{22}$, respectively
u, U_e	forward and trim forward speed in the body axes
V_x, V_z	horizontal and vertical speed
w, w_0	vertical velocity in the body and inertial axes
W_e	trim vertical speed in the body axes
x	state variable vector
X_q, X_u, X_w	X force derivatives
$X_{\theta_{is}}$	control derivative
Z_q, Z_u, Z_w	Z force derivatives
$Z_{\theta_{is}}$	control derivative
γ	flight-path angle
γ_d	desired deviated flight-path angle
η_1, η_2	maximum element of $\mathbf{A}_{11}$ and $\mathbf{A}_{22}$
θ	pitch angle
θ_0, θ_{ls}	main rotor collective and longitudinal cyclic input
Θ	trim pitch angle
λ_i	Eigenvalues of surge and pitch modes

Subscripts

e	equilibrium or trim point

Paper No. 3446. Manuscript received 8 April 2009, accepted 11 December 20.

https://doi.org/10.1017/S0001924000003882 Published online by Cambridge University Press

1.0 INTRODUCTION

Unintended adverse Interactions between an aircraft and its pilot, commonly described as pilot-induced oscillations or aircraft-pilot couplings (PIOs, APCs), have been investigated extensively since the Wright Brothers experienced such phenomena in their first powered flights[1-4]. Such dynamic couplings often occur when a pilot increases the gain in a closed loop task, working hard to achieve precision. Unfavourable, or adverse, APCs are often sudden or unexpected. It is often difficult to pinpoint the cause of such events and they may lead to extreme outcomes such as loss of control[5]. The term PIO is limited and, arguably, misleading since the coupling pattern between the aircraft and pilot can, in practice, be either oscillatory or aperiodic. The latter refers to situations where the excursions of aircraft motion diverge monotonically over time rather than oscillate. Therefore, the combined dynamics between the aircraft and the pilot are better described as APCs and the consequences as APC events[6,7]. If rotorcraft are considered, the couplings are described as rotorcraft-pilot-couplings (RPCs)[8-12], and are the subject of this paper.

It is well understood that A/RPC events may be triggered under a variety of circumstances, even though the nature of the event might itself be obscure. In Ref. 1, McRuer describes APCs in three categories:

- Cat. I governed by linear behaviour of the pilot and system. The couplings are often associated with high gain and increased time or phase delay effects.
- Cat. II typically involves limit cycle oscillations of the pilot-vehicle system due to nonlinear control elements in the feedback system, e.g. rate and position saturation.
- Cat. III covers severe pilot-vehicle oscillations, which are inherently non-linear and characterised by a transition from one transient response to another.

The search for robust design solutions that mitigate the adverse effects remains a research topic. The present paper addresses Cat. I RPCs, where the physical origins and design solutions are linked through an understanding of control strategy. Digital fly-by-wire flight control systems can, if not carefully designed, increase the potential for adverse interactions due to transport delays. Nonlinearities in rate and position limiter elements, flight-path or attitude constraints, or response type transition effects can also contribute to adverse couplings. Furthermore, pilot errors of judgement resulting from mildly adverse A/RPCs can contribute to the development of more severe A/RPC events.

Under high gain situations such as air-to-air refuelling, target tracking, operations in confined areas in poor visibility, or in the presence of disturbed atmospheric conditions, the aircraft needs to be flown with a degree of attitude and flight-path constraint[12,13]. Modern aircraft can be designed to deal with these kinds of situations through a stability and control augmentation system (SCAS). However, the coupled system – aircraft, SCAS, and pilot – may show unexpected stability characteristics such that strong control of one part of the system may drive another part unstable; hence the need to address this topic of 'stability under constraint' analytically.

The early pioneers in this field, Neumark[14] and Pinsker[15,16], investigated the problems of stability of fixed wing aircraft under constraint. Milne and Padfield[17] extended Neumark's and Pinsker's seminal work establishing a sound theoretical basis for such APCs using the theory of weakly coupled systems (WCS)[18], and forming an early foundation for the present work. In Ref. 19, Hodgkinson et al conducted a study to determine whether longitudinal, low-order, equivalent (linear) system parameters could be used to predict PIOs. In another study, Hess and Kalteis[20] employed the optimal control model to predict the susceptibility of an aircraft to longitudinal PIOs in pitch attitude tracking tasks, by providing a formal procedure for generating this form of pilot model.

In addition to the problems related to flight-path constraint, there exist specific practical difficulties for flight path control below the minimum drag speed[14,21,22]. Neumark[14] related the slope of the drag curve to problems of longitudinal stability. In this flight regime, as the speed decreases, so the drag increases which leads to a further reduction in speed. However, the natural modes (including the phugoid) are normally stable in this flight regime for the fixed-wing aircraft, and it is only under closed loop control that the surge mode is driven unstable in these low speed conditions.

The focus of the present study is an investigation of rotorcraft stability under flight-path constraint, with initial emphasis on situations where the use of collective pitch is restricted. In practice of course, it is normal, at low speed, for the pilot to adopt a strategy using collective for flight-path control and cyclic for attitude/speed control. The analysis that follows is therefore applicable to practical cases of partial power descents with a collective malfunction/restriction. The investigation aims to provide a theoretical framework for predicting a class of Cat. I RPC problems. The 'problem' is exercised on the FLIGHTLAB Bell 412, a model that has received a degree of validation at Liverpool[23], and ground-based and in-flight simulation tests have been conducted to support the theoretical developments. The stability of the closed-loop system is analysed by dividing the whole system into three sub-systems approximating the surge (forward speed) mode, the phugoid mode, and the heave (vertical speed) mode, using the theory of WCS[24,25]. The research forms part of the University of Liverpool's contribution to GARTEUR H-AG-16 (RPCs) involving a number of European Industry and Academic partners, aimed at providing more substantial design guidance for RPCs[26-28].

The paper is structured as follows: after the brief introduction to the theory and the problem in Sections 2 and 3, results from the 'exact' linear system are presented in Section 4 and the various partitioning levels using WCS theory are explored in Section 5, including a stability analysis of the surge and flight path motions. Finally, the results from piloted simulation on the HELIFLIGHT simulator at The University of Liverpool[29], and flight tests conducted at The National Research Council (NRC, Canada), are presented and discussed in Section 6.

2.0 THE THEORY OF WEAKLY COUPLED DYNAMIC SYSTEMS

A linear homogeneous aircraft dynamic system may be described by equations of the form;

$$\dot{x} = \mathbf{A}x \qquad \ldots (1)$$

where the vector $x \in R^I$ is the state variable vector and $\mathbf{A} \in R^{I \times I}$ is a square, real, and constant matrix. The system in Equations (1) is partitioned into the form as follows:

$$\begin{bmatrix} \dot{x}_1 \\ \dot{x}_2 \end{bmatrix} = \begin{bmatrix} \mathbf{A}_{11} & \mathbf{A}_{12} \\ \mathbf{A}_{21} & \mathbf{A}_{22} \end{bmatrix} \begin{bmatrix} x_1 \\ x_2 \end{bmatrix} \qquad \ldots (2)$$

where the vectors $x_1 \in R^m$ and $x_2 \in R^n$ are the sub state variable vectors, and the matrices $\mathbf{A}_{ij}$ have the corresponding dimensions. Particularly, let r and R stand for the maximum and minimum moduli of eigenvalues of the matrices $\mathbf{A}_{11}$ and $\mathbf{A}_{22}$, respectively. Let the eigenvalues of $\mathbf{A}_{11}$ lie on or within the circle of radius r and those of $\mathbf{A}_{22}$ lie without the circle of radius R.

A system can be described as weakly coupled if the following two conditions are satisfied:

$$r/R << 1 \qquad \ldots (3)$$

$$m\eta_1\eta_2/R^2 \leq 1 \qquad \ldots (4)$$

where η_1 and η_2 in Equations (4) are the maximum elements of $\mathbf{A}_{11}$ and $\mathbf{A}_{22}$ respectively. If these two conditions are met, then the eigenvalues of the system in Equations (1) can be approximated by the eigenvalues of the two matrices[12,30,31].

https://doi.org/10.1017/S0001924000003882 Published online by Cambridge University Press

$$\mathbf{A}_{11} = \mathbf{A}_{11} - \mathbf{A}_{12}\mathbf{A}_{22}\mathbf{A}_{21} \quad \ldots (5)$$

$$\mathbf{A}_{22} = \mathbf{A}_{22} \quad \ldots (6)$$

In addition, a similar process can be constructed for the three-level partitioning,

$$\begin{bmatrix} \dot{\boldsymbol{x}}_1 \\ \dot{\boldsymbol{x}}_2 \\ \dot{\boldsymbol{x}}_3 \end{bmatrix} = \begin{bmatrix} \mathbf{A}_{11} & \mathbf{A}_{12} & \mathbf{A}_{13} \\ \mathbf{A}_{21} & \mathbf{A}_{22} & \mathbf{A}_{23} \\ \mathbf{A}_{31} & \mathbf{A}_{32} & \mathbf{A}_{33} \end{bmatrix} \begin{bmatrix} \boldsymbol{x}_1 \\ \boldsymbol{x}_2 \\ \boldsymbol{x}_3 \end{bmatrix} \quad \ldots (7)$$

so that the eigenvalues of the complete system can be approximated by the eigenvalues of the matrices.

$$\mathbf{A}_{11}^{*} = \mathbf{A}_{11} - [\mathbf{A}_{12} \quad \mathbf{A}_{13}] \begin{bmatrix} \mathbf{A}_{22} & \mathbf{A}_{23} \\ \mathbf{A}_{32} & \mathbf{A}_{33} \end{bmatrix}^{-1} \begin{bmatrix} \mathbf{A}_{21} \\ \mathbf{A}_{31} \end{bmatrix} \quad \ldots (8)$$

$$\mathbf{A}_{22}^{*} = \mathbf{A}_{22} - \mathbf{A}_{23}\mathbf{A}_{33}^{-1}\mathbf{A}_{32} \quad \ldots (9)$$

$$\mathbf{A}_{33}^{*} = \mathbf{A}_{33} \quad \ldots (10)$$

These approximations will form the basis of the search for analytic solutions to RPC Cat. I problems.

3.0 FLIGHT-PATH CONSTRAINT IN THE VERTICAL PLANE

The linearised equations of helicopter motion from rectilinear flight can be written in the form shown in Equations (11)[12].

$$\frac{\mathrm{d}}{\mathrm{d}t}\begin{bmatrix} u \\ w \\ q \\ \theta \end{bmatrix} = \begin{bmatrix} X_u & X_w & X_q - W_e & -g\mathrm{Cos}\Theta_e \\ Z_u & Z_w & Z_q + U_e & -g\mathrm{Sin}\Theta_e \\ M_u & M_w & M_q & 0 \\ 0 & 0 & 1 & 0 \end{bmatrix} \begin{bmatrix} u \\ w \\ q \\ \theta \end{bmatrix} + \begin{bmatrix} X_{\theta_{ls}} \\ Z_{\theta_{ls}} \\ M_{\theta_{ls}} \\ 0 \end{bmatrix} \theta_{ls} \quad \ldots (11)$$

The vertical velocity w_0 referenced to the Earth axis is given by the expression in Equations (12).

$$w_0 = w - U_e\theta \quad \ldots (12)$$

Transforming Equations (11) to include the vertical velocity state variable gives Equations (13).

$$\frac{\mathrm{d}}{\mathrm{d}t}\begin{bmatrix} u \\ w_0 \\ w \\ q \end{bmatrix} = \begin{bmatrix} X_u & g\mathrm{Cos}\Theta_e/U_e & X_w - g\mathrm{Cos}\Theta_e/U_e & X_q - W_e \\ Z_u & g\mathrm{Sin}\Theta_e/U_e & Z_w - g\mathrm{Sin}\Theta_e/U_e & Z_q \\ Z_u & g\mathrm{Sin}\Theta_e/U_e & Z_w - g\mathrm{Sin}\Theta_e/U_e & Z_q + U_e \\ M_u & 0 & M_w & M_q \end{bmatrix} \begin{bmatrix} u \\ w_0 \\ w \\ q \end{bmatrix} + \begin{bmatrix} X_{\theta_{ls}} \\ Z_{\theta_{ls}} \\ Z_{\theta_{ls}} \\ M_{\theta_{ls}} \end{bmatrix} \theta_{ls} \quad \ldots (13)$$

This transformation allows an investigation of flight-path and vertical velocity control to be more easily undertaken. In addition, proportional pilot feedback control between vertical velocity and longitudinal cyclic can be written as the control law shown in Equations (14).

$$\theta_{ls} = k_{w0}w_0 \ (k_{w0} > 0 \text{ for stabilising control}) \quad \ldots (14)$$

After rearranging, the longitudinal equations can be written in the form described in Equations (15).

$$\frac{\mathrm{d}}{\mathrm{d}t}\begin{bmatrix} u \\ w_0 \\ w \\ q \end{bmatrix} = \begin{bmatrix} X_u & g\mathrm{Cos}\Theta_e/U_e & X_w - g\mathrm{Cos}\Theta_e/U_e & X_q - W_e \\ Z_u & g\mathrm{Sin}\Theta_e/U_e & Z_w - g\mathrm{Sin}\Theta_e/U_e & Z_q \\ Z_u & g\mathrm{Sin}\Theta_e/U_e & Z_w - g\mathrm{Sin}\Theta_e/U_e & Z_q + U_e \\ M_u & 0 & M_w & M_q \end{bmatrix} \begin{bmatrix} u \\ w_0 \\ w \\ q \end{bmatrix} + \begin{bmatrix} X_{\theta_{ls}} \\ Z_{\theta_{ls}} \\ Z_{\theta_{ls}} \\ M_{\theta_{ls}} \end{bmatrix} \theta_{ls} \quad \ldots (15)$$

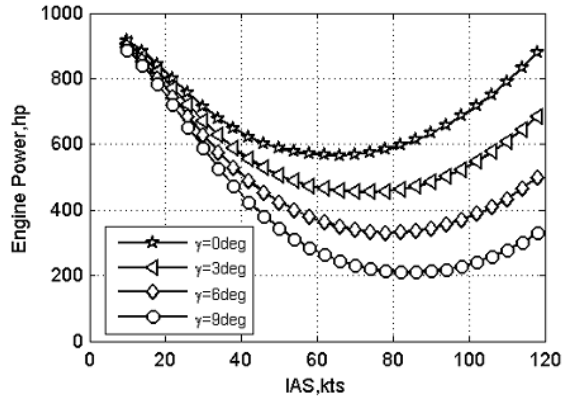


Figure 1. Power *vs* indicated air speed (IAS) for FLIGHTLAB Bell 412 with various flight-path angles.

4.0 ROOT LOCI FROM THE 'EXACT' SYSTEM

Based on the power curves in Fig. 1, the cases investigated include various combinations of trimmed forward speeds V_x = 20 to 50kt, and descending speeds V_z = 0, 5, 10, and 15kt. In addition, the feedback gain values (k_{w_0}, deg/(ms^{-1})) vary from zero to infinity. The basis of comparisons will be the eigenvalues of the 'exact' system matrix, given in Equations (15). Because of the similarities of the results, only two typical cases with V_x = 30kt and V_x = 50kt, are shown in Figs 2 and 3.

The root loci for the three modes – the phugoid mode, the surge and heave modes, are shown in Figs 2 and 3. These descriptors are maintained in the following discussion, even though it is recognised that the modes change shape as the feedback gain is increased. For the same forward speed, the root loci of the phugoid mode are shifted further left (more stable) as the descent speed increases. The mode tends to be controlled more effectively when the descent speed is higher. For example, the phugoid mode in Fig. 3(c) is completely stabilised. In addition, the phugoid mode is located further right (more unstable) as the forward speed increases. The curves of the phugoid mode in Fig. 2(a) and Fig. 3(a) also show a curious phenomenon, in that they are initially stabilised by the control, but lose stability again as the gain increases, only to re-stabilise at high gain conditions. Therefore, in some conditions there are three intersecting points on the imaginary axis. The stability of the surge mode also decreases as pilot gain is increased. The locus of this mode moves further right as the descending speed increases for the same forward speed. Moreover, the loci move further left as the forward speed increases. Finally, all cases show that the vertical heave speed mode remains stable, demonstrating the effectiveness of the feedback control. However, the control has driven the 'uncontrolled' states into various degrees of instability, with potential for exposing a classical RPC.

The critical gain values corresponding to the phugoid mode changing stability are shown in Table 1 and Table 2. Table 1 shows the critical gains for level flight cases that generally have three intersecting points on the imaginary axis. As shown, the gain values of the first intersecting point (K_1) are all less than 0·1 deg/(ms^{-1}) indicating that a very small gain value can make the phugoid mode stable. In Table 2, results for the descending flight cases are shown. Compared with level flight, the situation is more straightforward, since all curves are wholly located on the left-half plane, or only have one intersecting point with the imaginary axis; an exception is the case of V_x = 50kt and V_z = 5kt that has three crossing points as noted in Table 2. Moreover, even the gain values of the cases with the single intersecting point are also all less than 0·1deg/(ms^{-1}).

https://doi.org/10.1017/S0001924000003882 Published online by Cambridge University Press

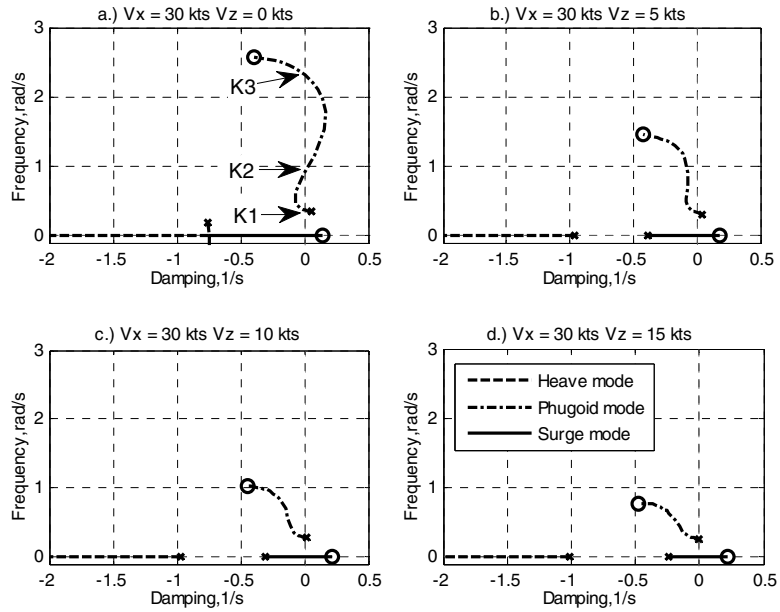


Figure 2. Root loci with V_z feedback (exact matrix calculation); V_x = 30kt *x* – poles; o – zeros; $K_{1\text{-}3}$ – crossing points with imaginary axis.

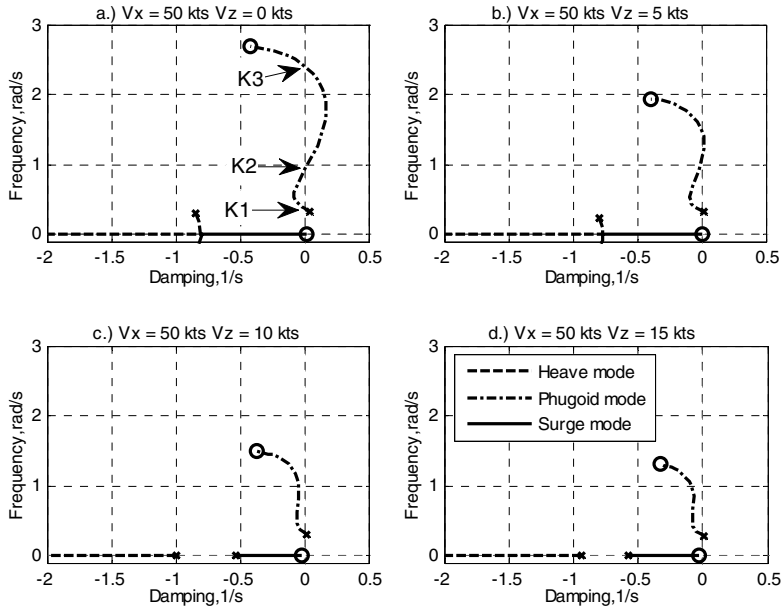


Figure 3. Root loci with V_z feedback (exact matrix calculation); V_x = 50kt *x* – poles; o – zeros; $k_{1\text{-}3}$ – crossing points with imaginary axis.

Table 1
Critical gains for the phugoid mode [deg/(ms^{-1})]

V_z/V_x	20kt	25kt	30kt	35kt	40kt	45kt	50kt
5kt	0·098	0·033	0·033	0·033	0·000	0·000	×
10kt	0·033	0·000	0·000	0·000	0·000	0·000	0·000
15kt	0·000	0·000	0·000	0·000	0·000	0·000	0·000

Note: means the initial point for the phugoid mode is located on the left-hand plane or neutrally stable

Table 2
Critical gains for the phugoid mode [deg/(ms^{-1})]

V_x (V_z = 0kt)	20kt	25kt	30kt	35kt	40kt	45kt	50kt
K_1	0·098	0·098	0·066	0·066	0·033	0·033	–
K_2	1·575	1·280	1·181	1·017	0·886	0·821	0·689
K_3	55·722	45·913	36·36	30·453	25·890	22·315	20·149

Note: × this case also has three critical gain values: 1.) 0·000 (neutral stable); 2.) 1·575; and 3.) 2·757

https://doi.org/10.1017/S0001924000003882 Published online by Cambridge University Press

Table 3
Critical gains for the surge mode [three-level partitioning, deg/(m s^{-1})]

$V_z \backslash V_x$	20kt	25kt	30kt	35kt	40kt	45kt	50kt
0kt	0·3941	0·4269	0·5254	0·6895	1·1161	2·4287	–
5kt	0·2200	0·2629	0·2629	0·3613	0·6895	1·7396	–
10kt	0·2200	0·1972	0·1644	0·2629	0·4598	–	–
15kt	0·2200	0·1644	0·1316	0·1316	0·4598	–	–

Note: in these cases the surge mode remains stable as the gain increases.

The results in Figs 2 and 3 show that when the feedback gain is large enough, the surge mode can be driven unstable. There thus exists a conflict between the control of the forward speed and pitch attitude under flight path constraint and, consequently, the gain value needs to be balanced. This represents a situation that can trigger a RPC. In the current application, the cyclic pitch is used to achieve both flight-path control and speed/attitude control. In practice, it is normal, at low speed, for the pilot to adopt a strategy using collective for flight-path control and cyclic for attitude/speed control. As noted in the Introduction, the analysis that follows is therefore applicable to practical cases of partial power descents with a collective malfunction. In Refs 14,32,33 the speed stability problem for a fixed-wing aircraft was attributed to strong control of the vertical speed when flying below the minimum drag speed. The root cause here is the non-minimum phase characteristic of flight-path control with elevator, combined with the fact that drag decreases as the speed increases (and vice-versa). A weakly coupled systems analysis, with different partitioning levels of the system dynamics, will be used to explain the curious behaviour of rotary-wing aircraft in the following Section.

5.0 ANALYSIS OF STABILITY USING DIFFERENT PARTITIONING LEVELS

5.1 Root loci from a three-level WCS

A three-level WCS analysis, introduced in Section 2, is used to partition Equations (15). The terms containing are ignored due their negligible contribution. The term $X_{\theta_{is}} k_{w_o}$ is also omitted because it has only a minor effect on the eigenvalue of Equations (15). The final expression adopted is shown in Equations (16).

$$\frac{\mathrm{d}}{\mathrm{d}t}\begin{bmatrix} u \\ w \\ q \\ w_0 \end{bmatrix} = \begin{bmatrix} X_u & X_w - g\mathrm{Cos}\Theta_e/U_e & X_q - W_e & g\mathrm{Cos}\Theta_e/U_e \\ Z_u & Z_w & U_e & Z_{\theta_{ls}} k_{w_0} \\ M_u & M_w & M_q & M_{\theta_{ls}} k_{w_0} \\ Z_u & Z_w & 0 & Z_{\theta_{ls}} k_{w_0} \end{bmatrix} \begin{bmatrix} u \\ w \\ q \\ w_0 \end{bmatrix} \quad \ldots (16)$$

The prerequisites of Equations (3) and Equations (4) need to be satisfied in order to adopt the three-level WCS. By checking Equations (16), these prerequisites can be met when k_{w_o} increases to a high value, i.e. strong control. This suggests that the three-level WCS is valid only for high gains. The cases portrayed below are the same as in Section 4, with two representative cases, V_x = 30kt and V_x = 50kt, illustrated in Figs 4 and 5.

The results shown in Figs 4 and 5 are clearly quite different from those in Figs 2 and 3. The first difference is the overlapping of the heave and surge mode loci, shown as the solid line between two poles on the damping axes. The second is that the phugoid mode is represented by the zero from the exact case. This phenomenon can be understood because of the prerequisites of Equations (3) and Equations (4) only being satisfied for high gain values and some parts of the heave and surge modes fail to be separated by the WCS.

The critical gain values of the surge mode from the three-level partitioning are shown in Table 3. The results in Table 3 show that as V_x increases, the gain value required to destabilise the surge mode also increases. For the case of V_x = 50kt and above, the surge mode remains practically stable.

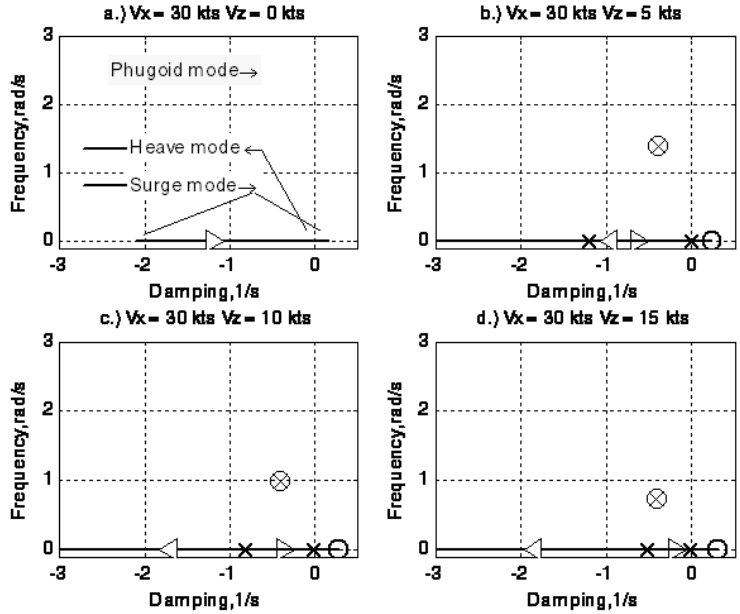


Figure 4. Root loci with V_z feedback (three-level approximation); V_x = 30kt *x* – poles; o – zeros.

https://doi.org/10.1017/S0001924000003882 Published online by Cambridge University Press

5.2 Stability of the surge mode

Equations (16), the simplified version of Equations (15), is also adopted for analysis in this section. Milne and Padfield[34] showed that the two-level partitioning, given in Equations (17), can be used to predict the low modulus speed mode.

$$\frac{\mathrm{d}}{\mathrm{d}t}\begin{bmatrix} u \\ w \\ q \\ w_0 \end{bmatrix} = \begin{bmatrix} X_u & X_w - g\mathrm{Cos}\Theta_e/U_e & X_q - W_e & g\mathrm{Cos}\Theta_e/U_e \\ Z_u & Z_w & U_e & Z_{\theta_{ls}} k_{w_0} \\ M_u & M_w & M_q & M_{\theta_{ls}} k_{w_0} \\ Z_u & Z_w & 0 & Z_{\theta_{ls}} k_{w_0} \end{bmatrix} \begin{bmatrix} u \\ w \\ q \\ w_0 \end{bmatrix} \quad \ldots (17)$$

The justification of this partitioning is quite straightforward. When k_{w_o} is large enough, as observed directly from $\mathbf{A}_{11}$ and $\mathbf{A}_{22}$ in Equations (17), then the requirements of Equations (3) and Equations (4) will be satisfied. After simplifying the partitioned expressions, the eigenvalue relating to the surge mode can written as,

$$\lambda_1 = X_u + \frac{g[M_u Z_w - Z_u(M_w + M_{\theta_{ls}} k_{w_0})]}{(M_w Z_{\theta_{ls}} - M_{\theta_{ls}} Z_w) U_e k_{w_0}} + \frac{X_w U_e(-M_u Z_{\theta_{ls}} + Z_u M_{\theta_{ls}}) + g M_u Z_{\theta_{ls}}}{(M_w Z_{\theta_{ls}} - M_{\theta_{ls}} Z_w) U_e} \quad \ldots (18)$$

Further simplification can be made by examining the relative magnitudes of the stability and control derivatives. For example, the direct derivatives $M_{\theta_{ls}}$ and Z_w are much more significant than $Z_{\theta_{ls}}$ and M_w. Hence, the following inequality is generally satisfied,

$$\left|M_{\theta_{ls}} Z_w\right| >> \left|M_w Z_{\theta_{ls}}\right| \quad \ldots (19)$$

For example, in the case of V_x = 45kt and V_z = 5kt, the value of $|M_{\theta_{ls}} Z_w|$ is two orders of magnitude larger than $|M_w Z_{\theta_{ls}}|$. In addition, the following two inequalities are also generally true,

$$\left|M_{\theta_{ls}} Z_w\right| >> \left|X_w(M_u Z_{\theta_{ls}} - Z_u M_{\theta_{ls}})\right| \quad \ldots (20)$$

$$\left|M_{\theta_{ls}} Z_w U_e\right| >> \left|g M_u Z_{\theta_{ls}}\right| \quad \ldots (21)$$

Applying these further approximations, Equations (18) can be reduced to the expression[12],

$$\lambda_1 = X_u - \frac{g[M_u Z_w - Z_u(M_w + M_{\theta_{ls}} k_{w_0})]}{M_{\theta_{ls}} Z_w U_e k_{w_0}} \quad \ldots (22)$$

For the surge mode to be stable, the condition $\lambda_1 < 0$ has to be satisfied. The force derivative Z_u is usually negative at low speed (thrust increases with speed perturbation). Therefore, $\lambda_1 < 0$ can be given by the following inequality,

$$X_u U_e Z_w k_{w_0} M_{\theta_{ls}} - g[M_u Z_w - Z_u(M_w + M_{\theta_{ls}} k_{w_0})] > 0 \quad \ldots (23)$$

Applying the further simplifications to establish the core effect,

$$\left|M_u Z_w\right| >> \left|Z_u M_w\right| \quad \ldots (24)$$

$$\left|\frac{g}{U_e} Z_u\right| >> \left|X_u Z_w\right| \quad \ldots (25)$$

Equations (23) can finally be rewritten as,

$$k_{w_0} < \frac{M_u Z_w}{Z_u M_{\theta_{ls}}} \quad \ldots (26)$$

In Ref. 13, the corresponding expression for the fixed-wing counterpart to Equations (22) is given by the approximation,

$$\lambda_2 \approx X_u + g\frac{Z_u M_w}{Z_w M_\eta} \quad \ldots (27)$$

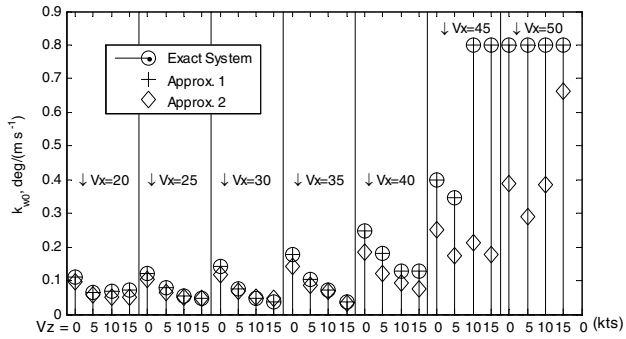


Figure 6. Comparison of the critical gain values from different approximations (k_{max}= 0·8°/(ms^{-1})).

The M_u effect is very strong at low speed for rotorcraft (caused by the flapping response to perturbations in u) but is negligible for subsonic fixed wing aircraft. The manner in which the stability problem develops is similar but the underlying physical effect quite different. In descending flight, the rotor downwash response to thrust changes increases to the point where the resultant thrust decreases, leading to an increased descent rate, following a collective input. The effect is described as power-settling in steep descent because of the marked effect on flight path. The zero for the approximate surge mode for fixed and rotary wing aircraft is the same, and given by Equations (27) (M_η replaced by $M_{\theta_{ls}}$).

The validity of the approximation given in Equations (26) can be established by comparison with the critical gain values calculated from the exact system (Equations (15)). The results are shown in Fig. 6.

In Fig. 6, the term k_{max} is the maximum gain value used to plot the figure, and the terms Approx. 1 and Approx. 2 refer to Equations (22) and Equations (26), respectively. This figure shows that the simple approximation (Equations (26)) predicts the stability boundary very well for forward speeds below 45kt, demonstrating the effectiveness of the two-level partitioning. However, at the higher speeds, the approximate predictions diverge from the exact values. Nevertheless, Equations (22) still remains a good approximation and consequently will be used in the more general analysis. In addition, these critical gain values are quite similar to the ones in Table 3 given by the three-level partitioning. This is understandable in that the surge mode depends on the u variable regardless of whether or not two-level or three level partitioning is used.

The speed instability is ultimately caused by the same effect as with fixed wing aircraft, although rotor downwash, rather than wing downwash, is the concern. In the speed range between hover and 50kt, the rotor inflow reduces at its sharpest rate with respect to airspeed increases[12]. A positive perturbation in forward speed therefore results in a reduction in inflow and an increase in rotor thrust. If the pilot pushes forward on the stick to increase descent rate, the speed increases and the increased thrust will eventually cause the aircraft to climb. The M_u effect complicates the situation since a positive speed perturbation causes the rotor disc to flap back and the helicopter to pitch up (this does not happen on fixed-wing aircraft), which tends to reduce the speed. This apparent speed stability is actually the cause of the phugoid instability and it is therefore no surprise that the stability of the surge and phugoid modes are linked under closed-loop control.

5.3 Stability of the phugoid mode

The loci of the phugoid mode in Figs 2(a) and 3(a) present a curious phenomenon in that they move back and forth in the complex plane. The approximations derived from the three-level partitioning predict the zero correctly. The multiple stability crossings, linked as discussed with the changing stability of the surge mode, are not

https://doi.org/10.1017/S0001924000003882 Published online by Cambridge University Press

predicted by either of these partitionings. Some insight into the problem can be gained from an examination of the combined medium and high modulus sub-systems in the three-level partitioning. The problem can then be approached qualitatively by focusing on three degrees of freedom (*u, w,* and *q*) as partitioned as

$$\frac{\mathrm{d}}{\mathrm{d}t}\begin{bmatrix} u \\ w \\ q \\ w_0 \end{bmatrix} = \begin{bmatrix} X_u & X_w - g\mathrm{Cos}\Theta_e/U_e & X_q - W_e & g\mathrm{Cos}\Theta_e/U_e \\ Z_u & Z_w & U_e & Z_{\theta_{ls}} k_{w_0} \\ M_u & M_w & M_q & M_{\theta_{ls}} k_{w_0} \\ Z_u & Z_w & 0 & Z_{\theta_{ls}} k_{w_0} \end{bmatrix} \begin{bmatrix} u \\ w \\ q \\ w_0 \end{bmatrix} \quad \ldots (28)$$

The large k_{w_o} values can guarantee this kind of two-level partitioning. After using Equations (5) and then rearrangement, the matrix for the combined phugoid and surge modes is given as follows.

$$\begin{bmatrix} X_u - 1/(k_{w_0} Z_{\theta_{ls}}) \cdot g/U_e Z_u & X_w - g/U_e - 1/(k_{w_0} Z_{\theta_{ls}}) \cdot g/U_e Z_w & X_q - W_e \\ 0 & 0 & U_e \\ M_u - 1/Z_{\theta_{ls}} \cdot M_{\theta_{ls}} Z_u & M_w - 1/Z_{\theta_{ls}} \cdot M_{\theta_{ls}} Z_w & M_q \end{bmatrix} \quad \ldots (29)$$

The associated characteristic equation can be written in the form,

$$a_3\lambda^3 + a_2\lambda^2 + a_1\lambda + a_0 = 0 \quad \ldots (30)$$

where a_0, a_1, a_2 and a_3 are functions of the stability and control derivatives. By applying the *Routh-Hurwitz* stability criteria[35] as follows,

$$\begin{array}{l|ll} s^3 & a_3 & a_1 \\ s^2 & a_2 & a_0 \\ s^1 & B & \\ s^0 & a_0 & \end{array} \quad \ldots (31)$$

the number of sign changes in the second column of Equations (31) will be the number of non-negative poles of the system in Equations (30). The expressions for a_0, a_1, a_2, a_2 and B can be;

$$a_3 = 1 \quad \ldots (32)$$

$$a_2 = -X_u - M_q + gZ_u/k_{w_o}Z_{\theta_{is}}U_e \quad \ldots (33)$$

$$a_2 \approx U_e M_{\theta_{is}} Z_w/Z_{\theta_{is}} - gZ_u/M_q/(k_{w_0} U_e Z_{\theta_{is}}) \quad \ldots (34)$$

$$a_2 \approx g_e M_{\theta_{is}} Z_u/Z_{\theta_{is}} + M_u g Z_w/(k_{w_0} Z_{\theta_{is}}) \quad \ldots (34)$$

and,

$$B = b_1 k_{w_o}^2 + b_2 k_{w_o} + b_3 \quad \ldots (36)$$

Equations (34) and (35) have been simplified as in Section 5.2. In Equations (36), where the denominator a_2 has been ignored, the terms b_1, b_2, and b_3 are also functions of the stability and control derivatives. Their simplified expressions are given as;

$$b_1 \approx (-X_u - M_q)\, M_{\theta_{is}} Z_w Z_{\theta_{is}} U_e^3 \quad \ldots (37)$$

$$b_2 \approx M_{\theta_{is}}\, gZ_u Z_w U_e^3 \quad \ldots (38)$$

$$b_3 \approx g^2 Z_u^2 M_q \quad \ldots (39)$$

The expressions in Equations (33) and (34) are always positive. Moreover, the condition to guarantee a positive a_0 is shown as follows,

$$k_{w_0} < \frac{M_u Z_w}{Z_u M_{\theta_{ls}}} \quad \ldots (40)$$

This expression is the same as that derived for the stability of the surge mode in Equations (26) – the sign of a_0 is related to the stability of the surge mode.

The matrix in Equations (29) consists of the surge and phugoid modes. Therefore, as far as the *Routh-Hurwitz* stability criteria are concerned, the stability variations, or the crossing of the imaginary axes of the phugoid mode, are contained in the sign changes of Equations (36). The sign variation can be analysed by the roots of Equations (36) or $\Delta = b_2^2 - 4b_1b_3$. After simplification, the Δ equation, or generalised damping, can be approximated as follows

$$\Delta' = -\mathrm{M}_{\theta_{is}} Z_w U_e + 4Z_{\theta_{is}}\, M_q^2 \quad \ldots (41)$$

In addition, the Δ' values of the all cases being investigated are plotted in Fig. 7. In Fig. 7, the data corresponding to $\Delta' > 0$ imply that the phugoid mode has two stability crossing points. The points corresponding to $\Delta' < 0$ imply that the phugoid mode has no crossing point. The locations of the points in Fig. 7 for all cases are consistent with the results presented in Figs 2 and 3. For instance, the case of V_x = 50kt has two points corresponding to $\Delta' > 0$ which represent V_z = 0kt and 5kt, respectively – Figs 3(a) and 3(b) show that there are, indeed, two crossing points. Overall, all these results are consistent with the derivation of Equations (41).

Assuming that Equations (36) (Equations (41) positive) has two different roots K_1 and K_2 ($K_1 < K_2$) for stability changes, the following observations can then be made.

$0 < k_{w_o} < k_1$, phugoid mode stable ... (42)

$k_1 < k_{w_o} < k_2$, phugoid mode unstable ... (43)

$k_{w_o} > k_2$, phugoid mode stable ... (44)

The consistency between Equations (40)/Fig. 6 and the original results shows the effectiveness of the applied WCS method. However, the primary drawback is that the method can only predict two stability crossings. Effectively, the initial point of the phugoid mode is assumed to be located in the stable plane. As a result, the

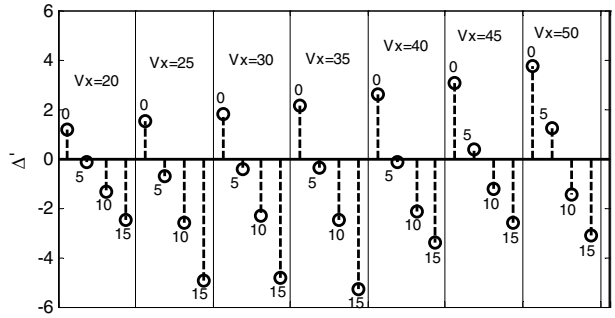


Figure 7. Illustration of the generalised damping values (Δ') to show stability of the phugoid mode.

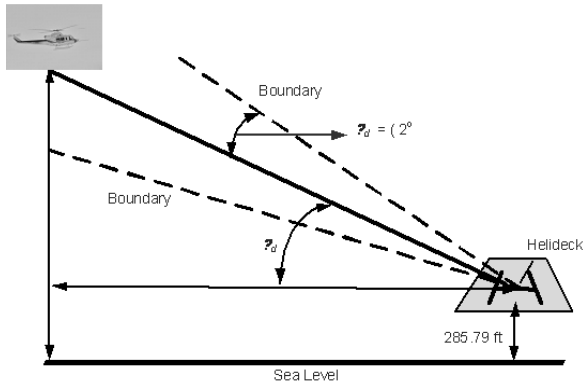


Figure 8. Trajectory for investigation of RPCs under flight-path constraint.

https://doi.org/10.1017/S0001924000003882 Published online by Cambridge University Press

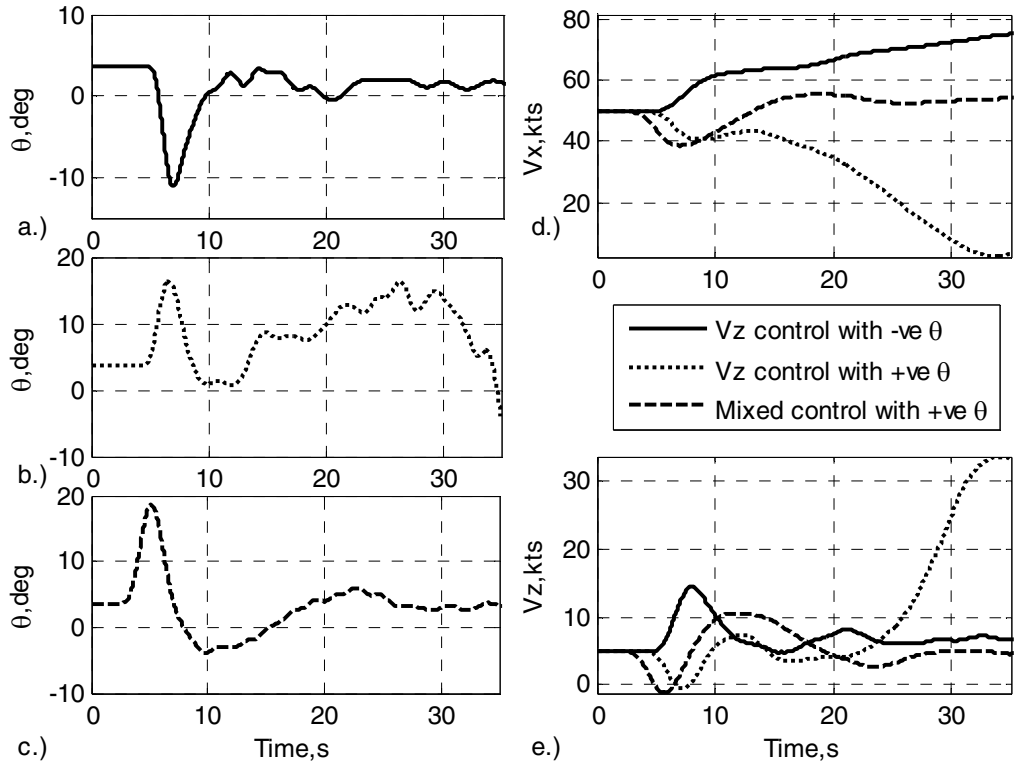


Figure 9. Results of the HELIFLIGHT simulation with longitudinal cyclic control only (V_x = 50kt and V_z = 5kt).

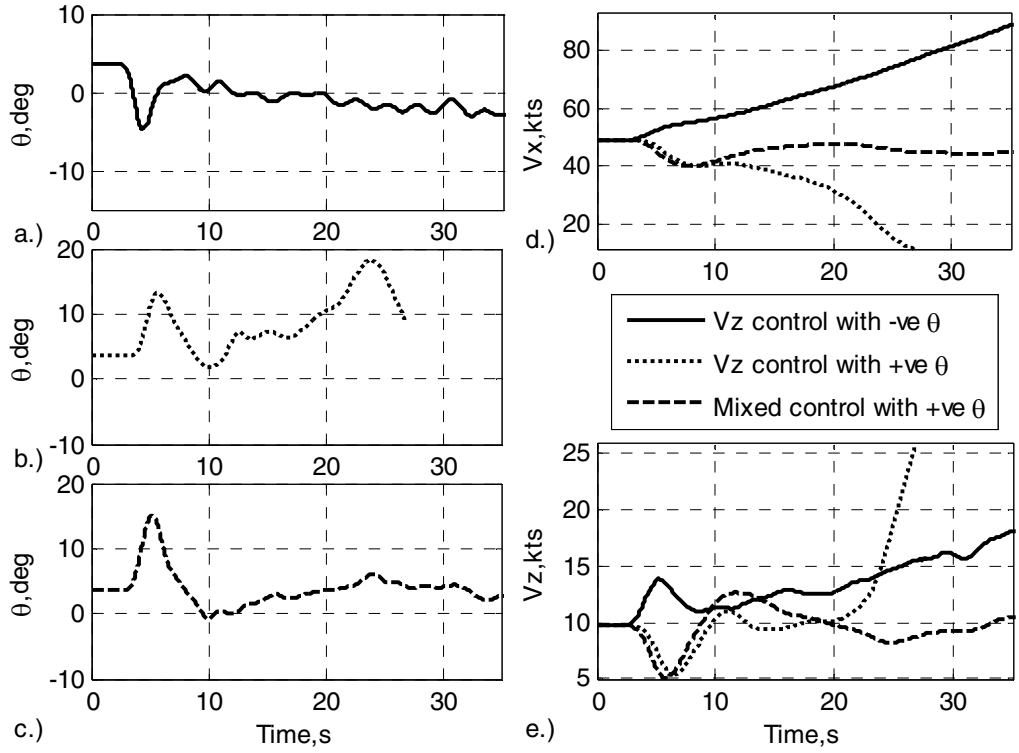


Figure 10. Results of the HELIFLIGHT simulation with longitudinal cyclic control only (V_x = 50kt and V_z = 10kt).

https://doi.org/10.1017/S0001924000003882 Published online by Cambridge University Press

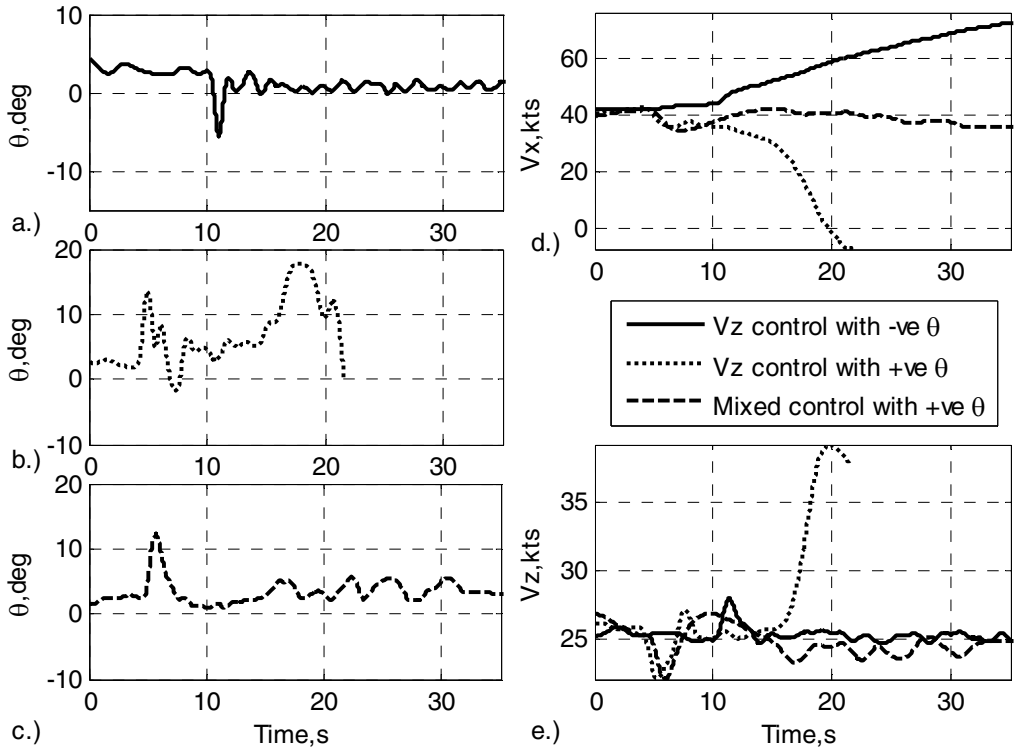


Figure 11. Results of the HELIFLIGHT simulation (autorotative flight).

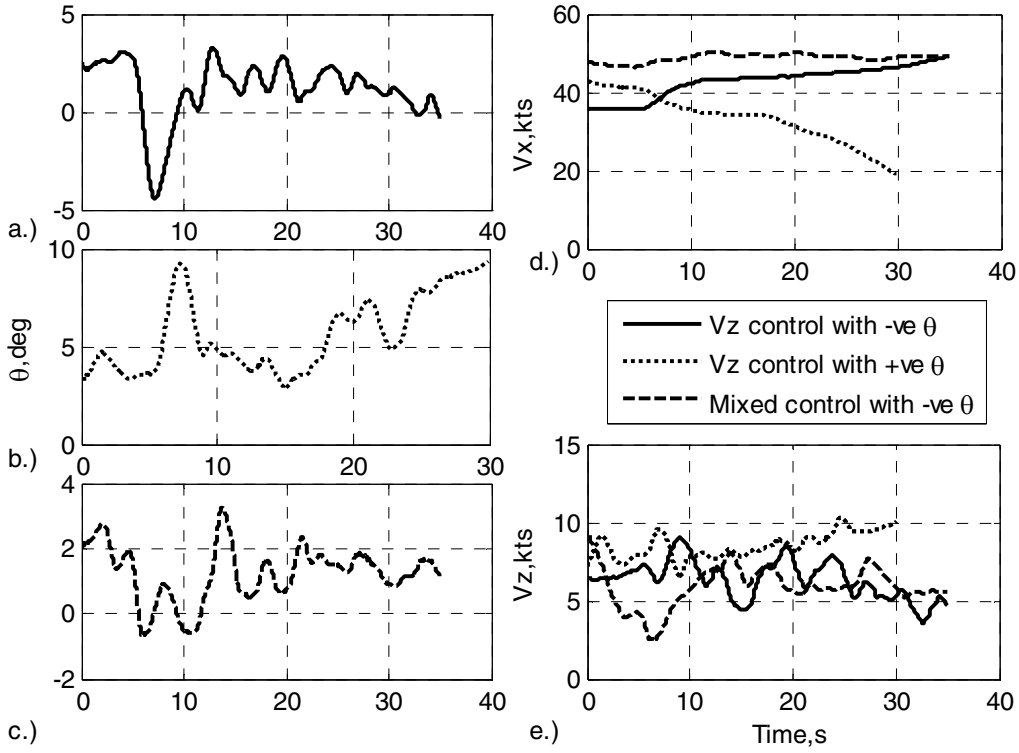


Figure 12. Results of the Bell 412 flight test with longitudinal cyclic control only.

https://doi.org/10.1017/S0001924000003882 Published online by Cambridge University Press

first stability change is ignored, although the corresponding gains are very small and thus it is still illuminating to apply this approach in practice. This statement can be reinforced by referring to the critical values for the phugoid mode from the 'exact' matrix, as shown in Table 1 and Table 2.

In addition, with strong control of the vertical velocity or flight-path, the modes dominated by the uncontrolled speed and pitch attitude motions are intimately linked. Referring to Equations (26), the larger the ratio M_u/Z_u, the higher the gain that can be used before the surge mode destabilises, but the earlier the phugoid mode transitions back into the unstable plane. For the case of the level flight case with V_x = 30kt, the gain value needed to guarantee surge mode stability is less than 0·2deg/(ms^{-1}), as shown in Fig. 6. In order to achieve the stability of the phugoid mode, the gain should be located within the range (0·0656, 1·1814) or alternatively a very high value that can be obtained by referring to Table 1. Therefore, the gain selected from the interval (0·0656, 0·2) will result in the combined system in Equations (28) being stable. The consequences of this complex interaction have been explored in exploratory piloted simulation and flight test trials and are discussed in the following Section.

6.0 PILOTED SIMULATION AND SUPPORTING FLIGHT TRIALS

6.1 Simulation objectives and mission task element

In Secs. 4 and 5, it was found that adverse RPCs and stability problems can arise from the conflict between attitude control and flight-path control in low speed flight, based on analysis of a linear longitudinal model. Moreover, as discussed, an appropriate feedback gain needs to be selected in order to guarantee the stability of both the surge and phugoid modes. In this Section, the relevance of these theoretical results to practical operations is investigated. A series of experiments have been conducted on the motion base HELIFLIGHT simulator at The University of Liverpool[36]. The simulation model used was the full nonlinear FLIGHTLAB Bell 412. A series of supporting flight tests have also been conducted on the Bell 412 research aircraft at the Flight Research Laboratory of the Canadian National Research Council (NRC).

As previously discussed, the normal piloting strategy at low speed is to use collective for flight-path control and cyclic for speed and attitude control. In the above analysis, only the longitudinal cyclic control is involved. Therefore, in both the HELIFLIGHT simulator and flight experiments, only the longitudinal cyclic was used to replicate the situation of collective restriction/malfunction. For the HELIFLIGHT experiments, the pilot(s) performed a series of approach-to-helideck profiles, with a pitch disturbance initiated during the manoeuvre. This allowed an investigation of the effect of different levels of task severity on pilot workload within defined performance standards. The test course is shown in Fig. 8. For the flight test, the Bell 412R was flown on a similar steep descending manoeuvre with initial altitude around 1,100ft and environment temperature –12 °C in a moderate breeze (13-17kt).

To fly the course successfully, the pilot has to maintain the flight path within the boundaries shown.

6.2 Analysis of results

Typical results from the HELIFLIGHT simulator trials are shown in Fig. 9 to Fig. 11 (≈50kt, 6º and 12º glide slopes, 50kt autorotation) and from flight tests in Fig. 12.

In all three ground-based simulation cases, results for three different situations are shown – a pitch down perturbation (*–ve* θ) with pilot controlling vertical velocity, a pitch up perturbation (*+ve* θ) with pilot controlling vertical velocity, and a pitch up perturbation with the pilot using a combined vertical velocity and horizontal velocity control strategy. Figure 9 corresponds to the 50kt partial power case with an initial glide slope of approximately 6º. Figure 10 shows the aircraft at 50kt with an initial glide slope of approximately 12º, and Fig. 11 shows the 50kt autorotation case with a descent rate of about 2,500ft/min. The pattern is similar in all three flight cases, including autorotation (it is recognised that the theoretical formulation above, with a constant rotor speed, does not fully reflect behaviour in autorotation and further investigation of this flight state will be included in the continuing research). With the pitch down perturbation, the pilot struggles to maintain rate of descent as the horizontal velocity component increases to more than 80kt. Following the pitch up perturbation, the horizontal velocity falls sharply and the pilot is soon unable to control the flight path as the rate of descent builds to over 30kt (≈3,000ft/min). Both of these cases are a consequence of the surge mode instability highlighted in Fig. 3. Strictly speaking, the linear approximation used to predict the behaviour in Fig. 3 breaks down when the velocity increases/decreases by more than a 'small' perturbation from the 50kt trim condition. It is hypothesised that the oscillatory cyclic control pattern at about 2rad/s, clear in Fig. 10 but less so in Fig. 9 and Fig. 11, reflects the pilot action in response to the poorly damped phugoid mode shown in Fig. 3.

In addition, a typical set of results from the Bell 412 flight trials for the same three situations are shown in Fig. 12. For these tests, the pilots performed a steep descending profile manoeuvre with different initial speeds, and they were also instructed to use cyclic only control strategy. All three cases in Fig. 12 show general consistency with the ground-based simulation results. For example, just after the pitch up perturbation, the forward velocity decreases abruptly to less than 20kt while the vertical speed is approximately held at 8kt. In contrast, with the pitch down perturbation, while the rate of descent is maintained roughly at 5kt, the forward speed rapidly increases.

As shown in Figs 9 to 12, by using a so-called 'mixed' control strategy, that combines control of the horizontal and vertical speeds, the pilot successfully maintains the flight condition. For the case of Fig. 10, to simulate a pitch disturbance, the pilot first initiates a positive pitch up perturbation by pulling the stick back (point A in Fig. 13), and the vertical and horizontal speeds consequently decrease. Moreover, the vertical speed decreases faster than the horizontal speed as shown in Fig. 10(d,e) in this phase. Therefore, the actual flight-path angle reduces, corresponding to the helicopter diverging from position A to position B in Fig. 13. The stick is then pushed forward and then quickly pulled back to the original trim position. As a result, both vertical and horizontal speeds increase with the vertical speed apparently increasing at a faster rate than the horizontal one. Hence, the helicopter moves to position C. The pilot then holds the stick for several seconds. This provides the opportunity for him to check the perturbations before applying further cyclic inputs. The pilot then slightly adjusts the control in an oscillatory fashion, the helicopter finally approaching position D, on the desired flight path.

As a footnote to the simple flight path analysis in this paper, the mixed control strategy has been briefly investigated by including both vertical and horizontal feedback into the control strategies, formulated in the control law,

$$\theta is = k_{V_z} V_z + k_{V_x} V_x \qquad \ldots (45)$$

According to the strategy that the pilot adopts, the vertical speed control is more significant than the horizontal speed, in that the flight-path angle is more sensitive to the variations in vertical speed. This can be approximately analysed taking a case from Fig. 3 (50kt), as shown in Fig. 14.

Figure 14, in which u is approximately equal to V_x, portrays the corresponding linear case with the mixed-control strategy of Fig. 9.

https://doi.org/10.1017/S0001924000003882 Published online by Cambridge University Press

The phugoid mode is unstable up to $k_{V_x} = 2$ deg/(ms^{-1}), but the related mode in Fig. 3 is initially stable, becoming neutrally stable within this feedback gain range (see Table 3). This can be interpreted as more 'workload' being required for the vertical speed control to guarantee the stability of the whole system. In addition, the pilot referred to using much lower gain in this case and, closing the loop on airspeed, found that control of vertical rate was sometimes 'counter-intuitive' – pushing to climb and vice-versa. This is illustrated in Figs 10(c) and 10(e) in which the stick has been pulled back slightly at 8s to try to reduce the flight-path angle. However, the vertical speed begins to decrease until around 12s. The non-minimum phase nature of vertical rate response to cyclic at low speed contributes to this effect, the corresponding linear model exhibiting a positive real zero.

This brief analysis of the mixed strategy will be developed further in the continuing research on this topic.

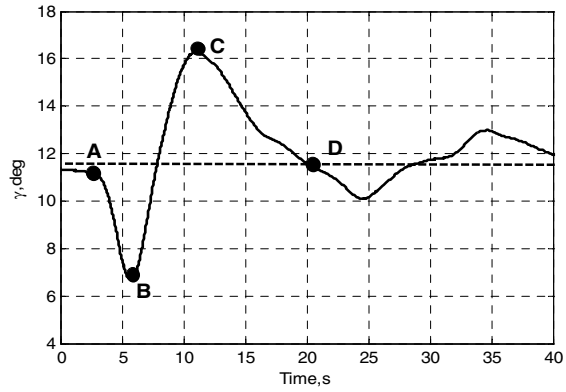


Figure 13. The flight-path angle variation during the simulation (expanded view from Fig. 10).

7.0 CONCLUSIONS AND RECOMMENDATIONS

Building on the foundation work of Ref. 12, the paper has reported an investigation of RPCs for descending flight situations with flight-path constraint. The weakly coupled system theory has been successfully adopted to facilitate understanding Cat. I RPC susceptibility under such flight-path constraint below the minimum-power speed. The research has found that RPC problems relate to the conflict between the control of the surge and phugoid modes when the vertical speed/flight path feedback gain increases. The approximation of the surge mode using a two-level partitioning method predicts the stability boundary for the low speed range, but the prediction degrades as the forward speed increases. Moreover, these results are similar to those obtained by the three-level partitioning method. In addition, the stability analysis using *Routh-Hurwitz* metrics has revealed the complex development of the phugoid stability under flight-path constraint.

The results from the piloted simulation trials in level flight, in powered descent, and in autorotation, to varying degrees, are consistent with the theoretical framework developed in this paper. The trials also show that the pilot was able to learn an effective, albeit non-intuitive, mixed control technique, to maintain the descent profile at low speed, even in autorotative flight. This mixed strategy has been briefly explored theoretically. Overall, there is a close analogy with the earlier predictions of speed stability for the fixed-wing aircraft flying below the minimum drag speed.

The 'problem' addressed in this research concerns a fairly limited area of normal operations and is of greatest concern in failure conditions or with control malfunctions. The continuing research on this topic will explore the, more successful, mixed control strategy further in addition to expanding the flight envelope to include autorotation and the consequences of rotor speed changes on the pilot-in the-loop dynamic and propensity to RPCs. The theoretical analysis presented also provides the framework for the development of handling qualities criteria in low speed descending flight. The speed instability experienced can be confusing to the pilot. It is recommended that consideration be given to this area in developing syllabi for pilot training in relevant emergency situations.

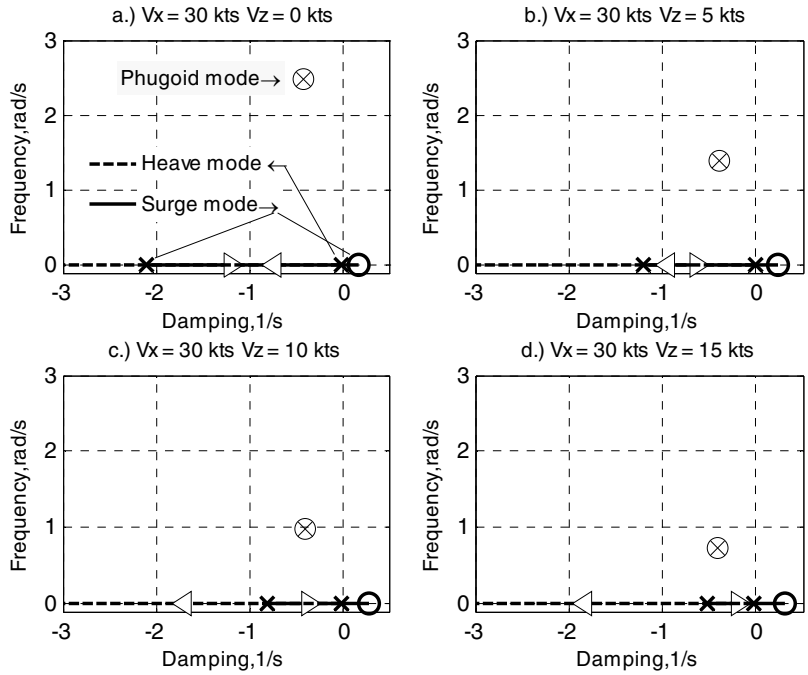


Figure 14. Root loci with *u* feedback (exact matrix calculation); V_x = 50kt *x* – poles; o – zeros.

https://doi.org/10.1017/S0001924000003882 Published online by Cambridge University Press

ACKNOWLEDGEMENTS

The research reported in this paper was funded by the UK Engineering and Physical Sciences Research Council grant EP/D003512/1 (Rotorcraft-Pilot Couplings). A version of the paper was presented at the RAeS/AHS international conference on 'Rotorcraft Handling Qualities', held in Liverpool, 3-5 November 2008. The study was also part of Liverpool's contribution to GARTEUR HC-AG16, Rotorcraft Pilot Couplings. The FLIGHTLAB Bell 412 simulation model was created and validated from data provided by the Flight Research Laboratory (FRL) of the Canadian National Research Council, Ottawa, as part of an ongoing collaboration in rotorcraft modelling, handling qualities and flight control. Grateful thanks are extended to the FRL team for their support, including hosting the flight trials in February 2009, and to the project test pilot, Andy Berryman, for his extensive contributions to this research.

REFERENCES

1. MCRUER, D.T. *et al Aviation Safety and Pilot Control Understanding and Preventing Unfavourable Pilot-Vehicle Interactions*, ASEB National Research Council, National Academy Press, Washington DC, USA, 1997.
2. MITCHELL, D.G. and KLYDE, D.H. Identifying a PIO signature – new techniques applied to an old problem, *J Guidance, Control and Dynamics*, January 2008, **31**, (1), pp 215-225.
3. KLYDE, D.H. and MITCHELL, D.G. Investigating the role of rate limiting in pilot-induced oscillations, *J Guidance, Control and Dynamics*, September 2004, **27**, (5), pp 804-813.
4. PADFIELD, G.D. and LAWRENCE, B. The birth of the practical aeroplane; an appraisal of the Wright Brothers' achievements in 1905, *Aeronaut J*, October 2005, **109**, (110), pp 421-438
5. SHAFER, M.F. and STEINMETZ, P. Pilot-induced oscillation research status at the end of the century, NASA Dryden Flight Research Center, Tech Rep, April 2001.
6. PAVEL, M.D. and PADFIELD, G.D. Understanding the peculiarities of rotorcraft-pilot couplings, Proc 64th Annual Forum of the American Helicopter Society, Montreal, Canada, May 2008.
7. LU, L and PADFIELD, G.D. The strongly controlled helicopter, 34th European Rotorcraft Forum, Liverpool, UK, 16 – 19 September 2008.
8. JUMP, M. *et al* Adverse rotorcraft-pilot coupling: test campaign development at the University of Liverpool, 34th European Rotorcraft Forum, Liverpool, UK, 16th – 19th September 2008.
9. WALDEN, R.B. A retrospective survey of pilot-structural coupling instabilities in naval rotorcraft, 63rd Annual Forum of the American Helicopter Society, Virginia Beach, VA, USA, 1 – 3 May 2007.
10. PADFIELD, G.D. *Helicopter Flight Dynamics*, 2nd ed, Blackwell Science, Oxford, UK, 2007.
11. NEUMARK, S. Problems of longitudinal stability below minimum drag speed, and theory of stability under constraint, Aeronautical Research Council, R&M 2983, HMSO London, July 1953.
12. PINSKER, W.J.G. Glide-path stability of an aircraft under speed constraint, Aeronautical Research Council, R&M 3705, HMSO London, February 1971.
13. PINSKER, W.J.G. Directional stability in flight with bank angle constraint as a condition defining a minimum acceptable value for Nv, RAE TR 67 127, June 1967.
14. MILNE, R.D. and PADFIELD, G.D. The strongly controlled aircraft, *Aeronautical Q*, May 1971, **XXII**, (2), pp 146-168.
15. MILNE, R.D. The analysis of weakly coupled dynamic systems, *Int J Control*, August 1965, **2**, pp 171-199.
16. HODGKINSON, J., GLESSNER, P.T., and MITCHELL, D.G. Prediction of longitudinal pilot-induced oscillations using a low order equation system approach, NASA/CP-2001-210389/VOL2, April 2004, pp 67-80.
17. HESS, R.A. and KALTEIS, R.M. Technique for predicting longitudinal pilot-induced oscillations, *J Guidance, Control and Dynamics*, 1991, **14**, (1), pp 198-204.
18. Anon, 2000. Aeronautical design standard performance specification handling qualities requirements for military rotorcraft ADS-33E-PRF. US Army Aviation and Missile Command, Aviation Engineering Directorate, Redstone Arsenal, Alabama, USA, March 2000.
19. MANIMALA, B.J. *et al* Rotorcraft simulation modelling and validation for control law design, *Aeronaut J*, February 2007, **111**, (1116), pp 77-88.
20. DIETERICH, O. *et al* Adverse rotorcraft-pilot coupling: recent research activities in Europe, 34th European Rotorcraft Forum, Liverpool, UK, 16 – 19 September 2008.
21. PAVEL, M.D. *et al* Adverse rotorcraft-pilot couplings – prediction and suppression of rigid body RPC, 34th European Rotorcraft Forum, Liverpool, UK, 16 – 19 September 2008.
22. PADFIELD, G.D. and WHITE, M.D. Flight simulation in academia; HELIFLIGHT in its first year of operation, *Aeronaut J*, September 2003, **107**, (1075), pp 529-538.
23. DUNCAN, W.J. *The Principles of the Control and Stability of Aircraft*, Cambridge University Press, 1952.

https://doi.org/10.1017/S0001924000003882 Published online by Cambridge University Press